

Received: 17 July 2024, Accepted: 27 August 2024

DOI: <https://doi.org/10.33282/rr.vx9i2.137>

SPATIOTEMPORAL ANALYSIS OF LAND USE LAND COVER AND THEIR IMPACTS ON LAND SURFACE TEMPERATURE OF DISTRICT SWAT, PAKISTAN

Fazal Haq¹, Muhammad Jamal Nasir², Anwar Saeed Khan³, Janas Khan⁴, Khalid Hussain⁵, Zahid Ali⁶

^{1&6}M.Phil. Scholars. Department of Geography & Geomatics, University of Peshawar
fazalhaq19960301@gmail.com, yasirktkgeo5@gmail.com

^{2&3}Assistant Professors, Department of Geography & Geomatics, University of Peshawar
drjamal@uop.edu.pk, asaeeed_geo@uop.edu.pk

^{4&5}PhD. Scholars. Department of Geography & Geomatics, University of Peshawar, khalidh953@gmail.com

⁶Assistant Professor, GD College, Akbarpura, Nowshera, Pakistan, azahidlec@gmail.com

Abstract

Land Use Land Cover (LULC) changes are among the most significant human-induced modifications to Earth's surface and immediate environment. In district Swat, rapid urbanization, population growth, deforestation, agricultural expansion, and increased built environment have altered LULC dynamics, leading to a rise in Land Surface Temperature (LST). This study aims to evaluate LULC variations and their impact on LST in the Swat district from 2002 to 2022. The analysis primarily utilizes satellite imagery from the USGS Earth Explorer website, covering the years 2002 (Landsat-5 TM), 2012 (Landsat-7 ETM), and 2022 (Landsat 9 OLI/TIRS). LST was derived using thermal band 6 for Landsat 5 TM and Landsat 7 ETM, and band 10 for Landsat 9 OLI/TIRS. The analysis suggests that agricultural land expanded from 577.6 km² to 1117.8 km² (2002-2022), built-up areas increased from 362.3 km² to 875.1 km² (2002-2022) and vegetation cover decreased from 1322.2 km² to 513.4 km² (2002-2022). Similarly, the snow cover reduced from 1567.2 km² to 953.6 km² (2002-2022) and water bodies shrunk from 405.0 km² to 292.4 km² (2002-2022). On the other hand, the LST analysis reveals that a significant increase of 12.49°C in maximum LST over the 20 years. This rise in LST is primarily attributed to the expansion of built-up areas, including houses, roads, and concrete structures, which tend to absorb more solar radiation. These findings highlight the substantial impact of LULC changes on the local climate in district Swat over the past two decades.

Keywords: *Satellite images, LST, LULC, solar radiation, built-up areas and agricultural land*

Introduction

The rapid expansion of urban areas accelerates land transformation processes and leads to swift increases in surface temperature over relatively brief periods (Guha et al., 2020; Nasir et al., 2022).

Land use refers to the human-driven conversion of natural environments into artificial landscapes, such as grasslands into industrial zones, residential areas, or agricultural fields (Roberts et al., 2015). Changes in land use and land cover (LULC) are considered among the most significant human-induced alterations to the Earth and its surrounding environment (Patra et al., 2018).

LULC changes result from complex interactions between various factors operating at both global scales (e.g., climate change, international markets) and local levels (e.g., topography, soil fertility, population growth) (Msofe, 2019; Negash et al., 2021). This transformation, driven by urbanization, has substantial negative impacts on both local and global environments (Khan et al., 2019). Furthermore, human-induced LULC alterations contribute to increases in land surface temperature (LST) (Rahaman et al., 2020; Song et al., 2018).

In the present day, LULC is changing at an unprecedented rate and intensity, surpassing any previous period in history (Namugize et al., 2018). Urban (built-up) areas, which constituted merely 3% of land cover in 1950, are projected to expand dramatically to 66% by 2050, driven by significant population growth and rural-to-urban migration patterns (Mohajerani et al., 2017). Land Surface Temperature (LST) is a measure of the heat emitted from the Earth's surface (Rajendran & Mani, 2015). It plays a crucial role as a climate variable intrinsically linked to global warming, while also serving as a key factor in local and regional surface energy and heat balance dynamics (Liu et al., 2021; Zou et al., 2020).

Among South Asian nations, Pakistan has undergone particularly rapid urbanization (Kedir et al., 2016). The effects of global warming are already manifesting in Pakistan through rising temperatures and alterations in land cover, posing numerous severe threats to the country (Amber and Knee, 2021). Reports indicate a significant expansion of built-up areas, from 3,969.04 hectares in 1998 to 6,147.06 hectares in 2018. Notably, Land Surface Temperature (LST) was observed to be higher in densely populated urban centers compared to surrounding rural areas. The LST for built-up regions increased from 42.8°C in 1998 to 46.9°C in 2018.

Research has revealed that the Swat district experienced a dramatic transformation over 40 years (1968-2007), with nearly 50% of its forest cover disappearing, giving way to a substantial increase in agricultural land and urban development (Qasim et al., 2013; Qasim et al., 2011). In light of

these trends, the current study aims to investigate the changes in land use and land cover patterns and their subsequent impact on land surface temperature in the Swat district over a two-decade period from 2002 to 2022.

Materials and Methods

Study Area

Swat is one of the districts in Khyber Pakhtunkhwa, province having a total area of 5,337 km². District Swat is geographically situated between 34° 30' to 35° 50' North latitude and 72° 10' to 73° 10' East longitude. The district Chitral is located in the North, Shangla district in the East, Malakand and Buner districts are located on the southern side and the Western side is bordered by districts Dir Lower and Dir Upper (Figure 1). Swat is the natural geographic area surrounded by River Swat. With an altitude ranging between 710 to 5910 meters above sea level and lush green forests, alpine pastures, and snow-clad mountains.

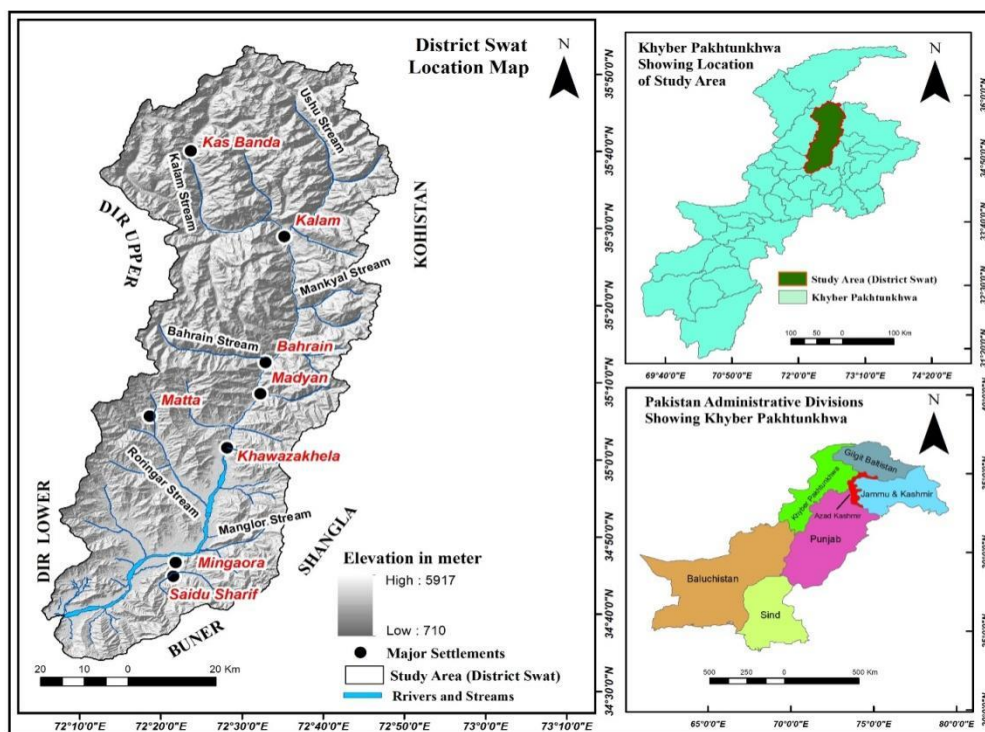


Figure 1: The location of study area map, district Swat

Data Sources

The study is mainly based on remote sensing data which was acquired from various sources. Landsat-5 TM, Landsat-7 ETM and Landsat 9 OLI/TIRS data for the years 2002, 2012 and 2022 was obtained from the USGS Earth Explorer website (<http://earthexplorer.com>). Landsat 5 Thematic Mapper (TM) of 2002, Landsat 7 Enhance Thematic Mapper Plus (ETM+) of 2012, and Landsat 9 Operational Land Imager and Thermal Infrared Sensor (OLI/TIS) of 2022 were used to produce the land use land cover (LULC) map of three periods. The Landsat images of three periods were also used to calculate the LST. The characteristics of Landsat-5 TM, Landsat-7 ETM, and Landsat 9 OLI/TIRS data are shown in Table 1.

Table 1 Remote Sensing Data Used in the Study Area

Date of acquisition	Sensor	Path/row	Thermal band	Spatial resolution	Source
05/26/2002	TM	151/35,36	6	30*30/120	USGS Earth Explorer
05/21/2012	ETM+	151/35,36	6	30*30/60	
05/17/2022	OLI/TIRS	151/35,36	10	30*30/100	

Source: <https://earthexplorer.usgs.gov/scene/metadata/full>

Image Preprocessing

Landsat image is helpful to provides information of the earth surface at various resolutions. Despite the challenges posed by low revisit frequency and cloud contamination (Zhou & Zhong, 2020), the acquired Landsat images (2002, 2012, and 2022) were enhanced through geometric and radiometric corrections to improve their quality. To ensure accurate analysis, a comprehensive pre-processing approach was employed. This included robust image registration techniques (Feng et al., 2019), image resampling via layer stacking (Islam et al., 2018), and atmospheric correction (Rani et al., 2017). These steps enabled the creation of high-quality images suitable for land use/land cover (LULC) change and land surface temperature (LST) analysis. The detailed methodology is illustrated in Figure 2.

LULC Change Analysis

The classification procedure was completed in the Arc GIS 10.8 environment using the maximum likelihood classifier approach from satellite images that have been obtained. The obtained images were categorized into different LULC classes including agricultural land, vegetation, barren land, built-up area, snow cover, and water bodies (Table 2).

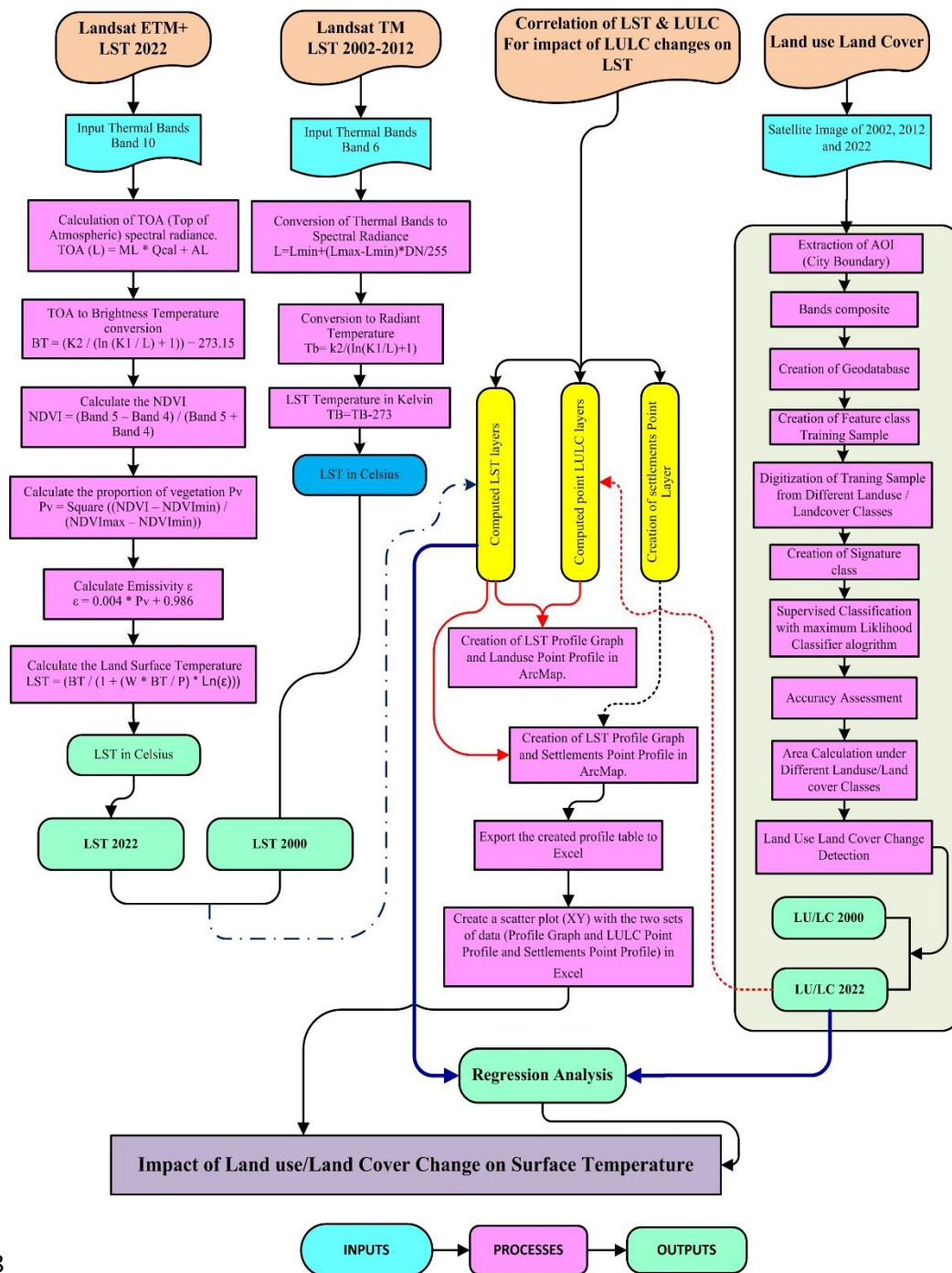


Figure 2: Illustrating objectives the suggested methodology employed to achieve the study

Table 2 Description of LULC classes used in the study area

LULC Classes	Description
Agricultural land	Areas used for cultivation, both annual and perennials crops
Vegetation	The area under forests and Plants is considered collectively.
Barren land	Areas with little or no vegetation cover, open lands, eroded gullies, and exposed rocks
Build-up area	Areas allotted for permanent residential, commercial areas, institutions and infrastructures
Snow	The solid form of water that precipitates from the atmosphere to the earth covers the earth permanently or temporarily.
Water bodies	Any significant accumulation of water on the surface of the earth in the form of lakes, streams, rivers, etc.

Accuracy assessment

Accuracy assessment is very crucial for measuring the effectiveness of an image during its classification. It is helpful to show the performance of a model regarding its weaknesses and strengths (Moisa et al., 2022). The Confusion matrix was applied to assess the accuracy of the classification. The confusion matrix consists of columns and rows representing the values and reality of classification from the ground (Chen & Zhang, 2017). The Kappa coefficient (Khat) measures the extent of agreement between two maps, taking into account all elements of the confusion matrix (Mishra et al., 2019), as expressed in Equation 1. Besides, the user accuracy, which was calculated as the ratio of correctly classified pixels to the total number of pixels in the same class, as described by Congalton (1991) in Equation 2, was also calculated. Producer accuracy was calculated as the ratio of correctly classified pixels to the total number of pixels in the same class, as explained by Disperati and Virdis (2015) in Equation 3. Furthermore, the overall accuracy was calculated to provide a comprehensive evaluation. The overall accuracy is the number of correctly classified pixels represented by diagonal lines of the error matrix (Equation 4) (Pouliot et al., 2014).

$$Khat = \frac{(Total * sum of the correct) - sum of all the (row total * column total)}{Total squared - sum of all the (row total * column total)} \dots\dots\dots (1)$$

$$User\ accuracy = \frac{Correctly\ classified\ pixels\ in\ a\ row}{Sum\ of\ all\ pixels\ in\ a\ row} * 100 \dots\dots\dots (2)$$

$$Producer\ accuracy = \frac{Correctly\ classified\ pixels\ in\ a\ class}{Sum\ of\ all\ the\ pixels\ in\ a\ column} * 100 \dots\dots\dots (3)$$

$$Overall\ accuracy = \frac{Sum\ of\ the\ correctly\ classified\ pixels}{Sum\ of\ all\ reference\ pixels} * 100 \dots\dots\dots (4)$$

LULC change detection

The magnitude of land use/land cover change was assessed based on three key factors: the amount of changed area, the extent of change, and the rate of change. Building on previous studies by Abraham et al. (2016), Abebe et al. (2019), and Elias et al. (2019), the rate of change was calculated using Equation 5 to quantify the magnitude of changes that occurred between the specified periods. This calculation provided valuable insights into the dynamics of land use/land cover transformations. This is also referred to as the Single land Use Dynamic Degree (SLUDD) developed by Liu, et al., (2002), and the Comprehensive Land Use Dynamic Degree (Xiulan, & Yuhai, (2011). The SLUDD can be calculated through Equation 5:

$$SLUDD = \frac{Ub - Ua}{Ua} \times \frac{1}{T} \times 100 \dots\dots\dots Eq. 5$$

*Where Ua is the area of land use type at the initial time (2002, 2012),
 Ub is the area of the that land use type at the later time (2012 and 2022)
 T is the gap between initial time and later*

According to Quan et al., (2015) it is a measure of the variation of conversion of land use land cover class into other LULC classes. They referred to SLUDD as an appropriate measure of the percentage annual change in particular land use land cover class.

Retrieval of LST

The Land Surface Temperature (LST) was calculated using Landsat Thermal Infrared (TIR) imagery. Specifically, band 6 was utilized for Landsat 5 Thematic Mapper (TM) and Landsat 7 Enhanced Thematic Mapper Plus (ETM+), while band 10 was used for Landsat 9 Operational Land

Imager/Thermal Infrared Sensor (OLI/TIRS) satellite images. These sensors captured the heat emitted from the Earth's surface, providing thermal data in the form of digital numbers (DN). According to Dener and Alves (2016), these DN values can be converted to brightness temperature, and radiance, enabling the calculation of LST from remotely sensed satellite data.

Conversion of Digital Numbers to top of Atmosphere (TOA) Spectral Radiance

Digital number (DN) stores thermal data in the Landsat sensor and deliver a manner of representing signifying pixels that have not yet been calibrated and converted into radiance units (Aik et al., 2020). To calculate, LST (Eq. 6) is the first process that must be followed for Landsat 8 Thermal infrared sensor TIRS to convert DN to radiance.

$$L\lambda = (ML * Q \text{ Cal}) + AL \dots \dots \dots (6)$$

Where “Lλ” represents the top of atmosphere (TOA) spectral radiance (Wm⁻² sr⁻¹µm⁻¹). ML is the band-specific multiplicative rescaling factor from the metadata (Radiance_mult_band x, where x is the band number). AL is the band-specific additive rescaling factor from the metadata (Radiance_add_band x, where x is the band number). Q Cal is the quantized calibrated standard product pixel values (DN).

For converting the Digital number (DN) to radiance (Eq. 7 and 8) for Landsat 5TM and Landsat 7ETM+, the gain and bias method was used (citation).

$$L\lambda = \text{gain} * Q\text{cal} + \text{bias} \dots \dots \dots (7)$$

$$\text{Radiance} = \frac{L_{max} - L_{min}}{QCAL_{Max} - QCAL_{min}} \times (QCAL - QCAL_{min}) + L_{min} \dots \dots \dots (8)$$

Where,

$$L_{MAX} = \text{Radiance Maximum Band 6} = 15.303$$

$$L_{MIN} = \text{Radiance Minimum Band 6} = 1.238$$

$$QCAL_{MAX} = \text{Quantize CAL Maximum Band 6} = 255$$

$$QCAL_{MIN} = \text{Quantize CAL Minimum Band 6} = 1$$

Conversion of Radiance to Brightness Temperature

After the DN's are converted to radiance, the thermal band's spectral radiance should be converted to brightness temperature (Eq. 9). This is usually accomplished using thermal constants delivered in the metadata file (Aik et al., 2020).

$$BT = K2 + \ln\left(\frac{K1}{LY} + 1\right) - 273.15 \dots \dots \dots 9$$

BT = Brightness temperature

LY = Spectral Radiance in watts (meter square)

K1 = Calibration Constant 1 (607.76)

K2 = Calibration Constant 2 (1260.56)

Land Surface Emissivity Estimation using NDVI

The NDVI was used to categorize the distribution of vegetation cover and their greenness as well. Consequently, it also explores the transformation of NDVI into values associated with the cover portion using empirical relationships with vegetation indexes as possible basis functions (Tomar et al., 2013).

NDVI is calculated using Eq. 10

$$NDVI = \frac{NIR-R}{NIR+R} \dots \dots \dots (10)$$

Where NDVI is the normalized difference Vegetation Index, NIR is the near-infrared band and R is the red band. From the NDVI values acquired, the next step in obtaining Land Surface Emissivity (LSE), mainly the calculation of the proportion of vegetation index (Pv), was achieved.

Calculating the Proportion of Vegetation (Pv)

The proportion of vegetation (Pv) is calculated according to Eq. 11

$$PV = \left(\frac{NDVI-NDVImin}{NDVImax-NDVImin}\right)^2 \dots \dots \dots (11)$$

Where Pv represents the proportion of vegetation, which is calculated according to Eq. 11.

Land Surface Emissivity (LSE) Assessment

Land surface emissivity (ϵ) is significant to estimates of LST because Dutta (2015) and Ogunode (2017) the proportionality factor to predict emitted radiance and represents the efficiency of

transmitting thermal energy across the surface into the atmosphere represented by land surface emissivity. Sobrino et al., (2004) state that the emissivity is calculated using (Eq. 12).

$$\varepsilon = 0.004PV + 0.986 \text{ ----- (12)}$$

The calculated radiant surface temperature will be corrected for emissivity using Eq. 13

$$LST = \left(\frac{BT}{1 + \left(\frac{\lambda BT}{\rho} \right) \times \ln(\varepsilon \lambda)} \right) - 273.15 \text{Eq 13}$$

Where LST is the land surface temperature (in Kelvin); and TB is the radiant surface temperature (in Kelvin). λ is the wavelength of emitted radiance (11.5 μm). ρ is $h \times c/\sigma$ (1.438×10^{-2} mK); h is the Plank's constant (6.26×10^{-34} J s); c is the velocity of light (2.998×10^8 m/s); σ is Stefan Boltzmann's constant (1.38×10^{-23} J K⁻¹); and ε is the land surface emissivity.

Result and Discussion

LULC Change Analysis

The major change in LULC was detected by using the method of Maximum Likelihood classification. LULC was classified into six different classes i.e. vegetation cover, agricultural land, barren land, water bodies, snow cover, and build-up area for the three periods of 2002, 2012, and 2022 as shown in Table 4. Agricultural land dominates the most as compared to other LULC classes which cover 577.6 km², 940 km² and 1117.8 km² for the years 2002, 2012, and 2022 respectively. On the other hand, vegetation cover shows a high decline in area due to expansion in agricultural land which is supported by Tezera et al. (2015) and Ebabu et al. (2019). Moreover, it is observed that the reduction in forest land may be the degradation of forests because cultivated land expansion as a consequence of rapid population growth is favored by (Olika & Iticha, 2019)

LULC Change Matrix

In this research study, the maximum likelihood classification was used to identify LULC change from 2002 - 2022. Major conversion of different LULC changes in district Swat is depicted in Table 4 and Figure 3. The change in LULC was calculated for vegetation cover which converted to agricultural land by 61.1% (808.8 km²). The classification of land use/land cover (LULC) change images highlights significant transformations between 2002 and 2022. The most prominent change was the conversion of forest land to agricultural land. Additionally, snow cover decreased

substantially, from 1567.2 km² in 2002 to 953.6 km² in 2022, resulting in a net loss of 613.6 km². Furthermore, the area under water also showed a decline, decreasing from 405 km² to 292.4 km², representing a loss of 112 km² over the study period.

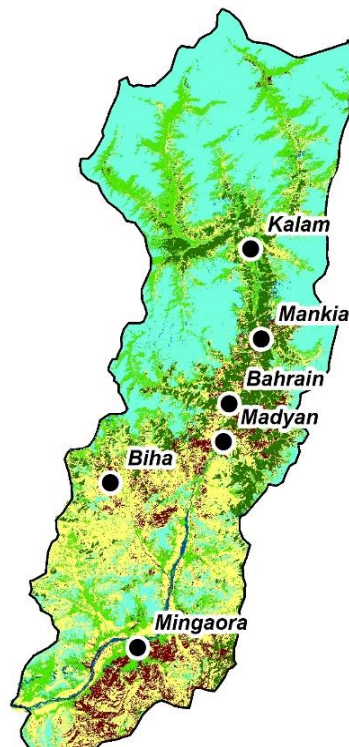
Table 3: District Swat Land Use Land Cover Change, (2002-2022)

Land use	Area (Km ²) (2002)	Area (Km ²) (2012)	Area (Km ²) (2022)	Change (2002-2022)
Agricultural land	577.6	940	1117.8	540.2
Vegetation	1322.2	695.8	513.4	-808.8
Barren land	1102.7	1493.4	1585.2	482.5
Built-up area	362.3	735.2	875.1	612.8
Snow	1567.2	1127.5	953.6	-613.6
Water bodies	405.0	345.6	292.4	-112.6
Total	5.337	5.337	5.337	

A District Swat Land use Land Cover 2002



B District Swat Land use Land Cover 2012



C District Swat Land use Land Cover 2022

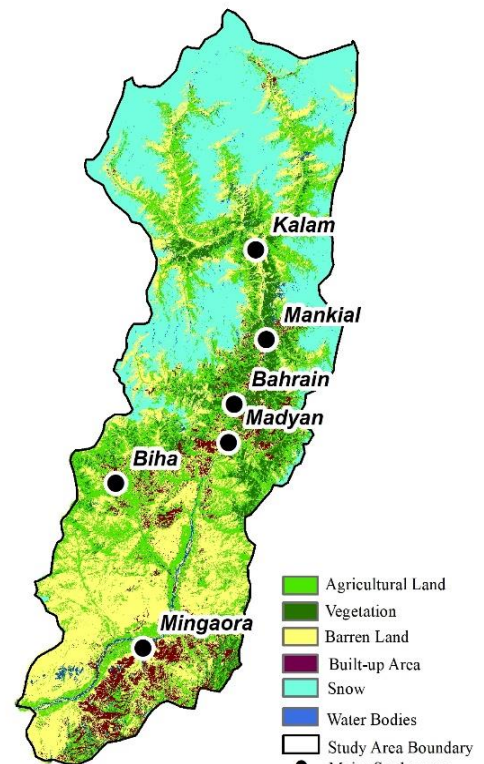


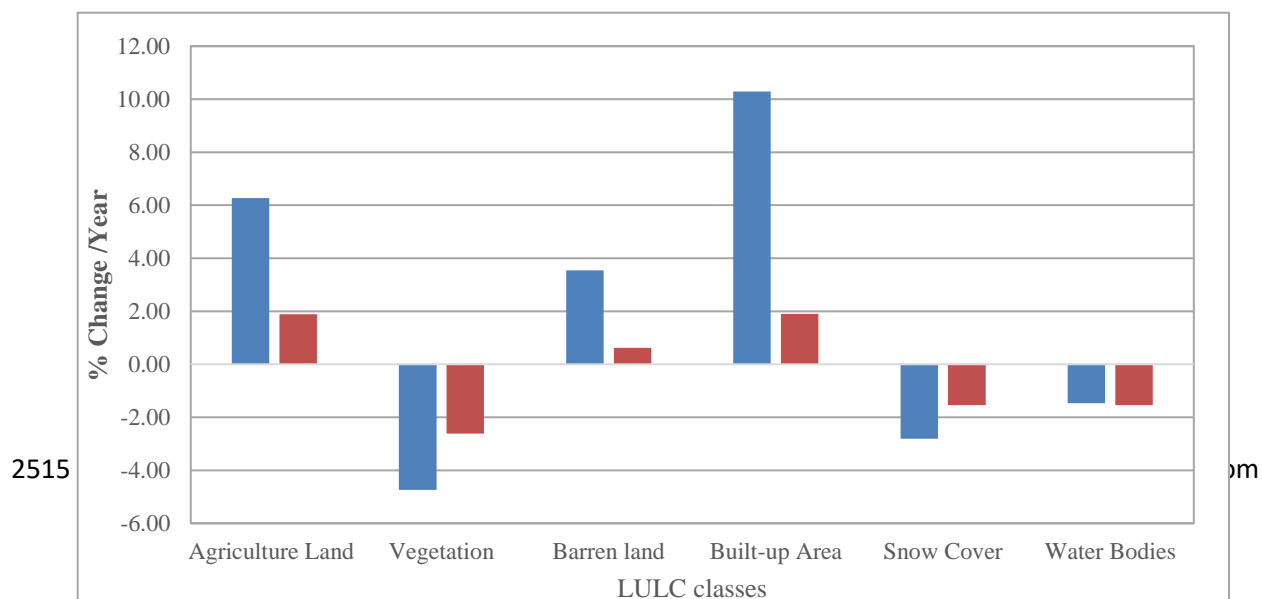
Figure 3A shows the LULC of 2002, 3B illustrates the LULC of 2012, and 3C highlights LULC of 2022 of district Swat.

Rate of LULC Change

Table 4 summarizes the analysis results, showing the Single Land Use Dynamic Degree (SLUDD) dynamics for the period between 2002-2022. The analysis reveals that between 2002 and 2022, significant land use changes were observed. The built-up areas increased by 10.29% annually between 2002-2012 and 1.90%/year during 2012-2022. The increase in built-up area was rapid during 2002-2012 as compared to 2012-2020. Agricultural land increased by approximately 6.27% annually between 2002-2012 and 1.89% between 2012-2022. Conversely, the area under vegetation decreased by -4.74%/year during 2002-2012 and -2.62%/year during 2012-2020. This decline in vegetation cover is attributed to a corresponding increase in agricultural land and barren land. Similarly, the barren land increased by 3.54% and 0.61% annually between 2002-2012 and 2012-2022 respectively. The snow cover also records a steady decrease between the two time periods (2002-2012 and 2012-2022) by -2.81% and -1.54% annually. A similar decrease was observed in waterbodies which decreased by -1.47% during 2002-2012 and by -1.54% between 2012-2022. This finding aligns with previous studies by Abebe et al. (2019) and Elias et al. (2019).

Table 4: District Swat Single Land Use Dynamic Degree (SLUDD), (2002-2022)

LULC	2002-2012 (%age)	2012-2022 (%age)
Agriculture Land	6.27	1.89
Vegetation	-4.74	-2.62
Barren land	3.54	0.61
Built-up Area	10.29	1.90
Snow Cover	-2.81	-1.54
Water Bodies	-1.47	-1.54



Accuracy Assessment

The accuracy assessment for each LULC class over the selected study period is shown in Table 5. The LULC accuracy assessment for 2002, 2012, and 2022 years produced an overall accuracy of 79.5%, 85.23%, and 72.78% respectively. The Kappa coefficient for the study periods were 57%, 62%, and 67% respectively. The analysis results demonstrate satisfactory results.

Table 5 Accuracy Assessment of LULC for 2002, 2012 and 2022

LULC types	2002		2012		2022	
	Producers' accuracy (%)	Users' accuracy (%)	Producers' accuracy (%)	Users' accuracy (%)	Producers' accuracy (%)	Users' accuracy (%)
Agricultural land	75	82.5	81	85.71	75.76	83.33
Vegetation	77.5	77.5	83.7	80	68.75	73.33
Barren land	80	80	82.4	80	68.97	66.67
Built-up area	85.7	75	87.5	88.57	64.71	73.33
Snow	76.2	80	90.9	85.71	75.00	70.00
Water bodies	84.6	82.5	86.4	91.41	87.50	70.00
Overall accuracy	79.5	-	85.23	-	72.78	-
Kappa coefficient	57	-	62	-	67	-

LST in response to LULC Change

The maximum LST observed in district Swat was 33.54 °C, 41.78 °C, and 46.03 °C for the years 2002, 2012, and 2022 respectively (Table 5). The mean LST in the year 2002 was about 16 °C and increased to 20.36 °C and 22.81 °C in 2012 and 2022 respectively. Results show that the southern part of the study area experienced high LST whereas the northeastern and northwestern parts of the study area experienced low LST (Figure 4A, 4B, and 4C). The highest LST was observed in

the low vegetation area, particularly around the build-up area and agricultural land. On the other hand, low LST has been found in areas dominated by forest land and snow cover. The LULC has a clear influence on LST. (Tan et al., 2020). Our results prove that areas with higher NDVI experienced lower LST, i.e. negative correlation. Thus, LULC has a significant effect on LST. (Guha & Govil, 2020; Kumar & Shekhar, 2015). LULC change and unwise use of natural resources are the key driving forces for the increasing trends of maximum temperature.

LST can be significantly impacted by the presence or lack of greenery. Forest cover, including trees and plants, offers shade, transpires water, and cools the region around them. Due to diminished cooling effects, regions with less greenery have greater LST. LST is influenced by the topography, including elevation, aspect, and slope. Low atmospheric pressure, which absorbs less of the earth's radiation's outgoing rays, causes high altitudes to have lower LST. In contrast, low-lying places like valleys absorb more solar radiation due to a high air density, which raises LST.

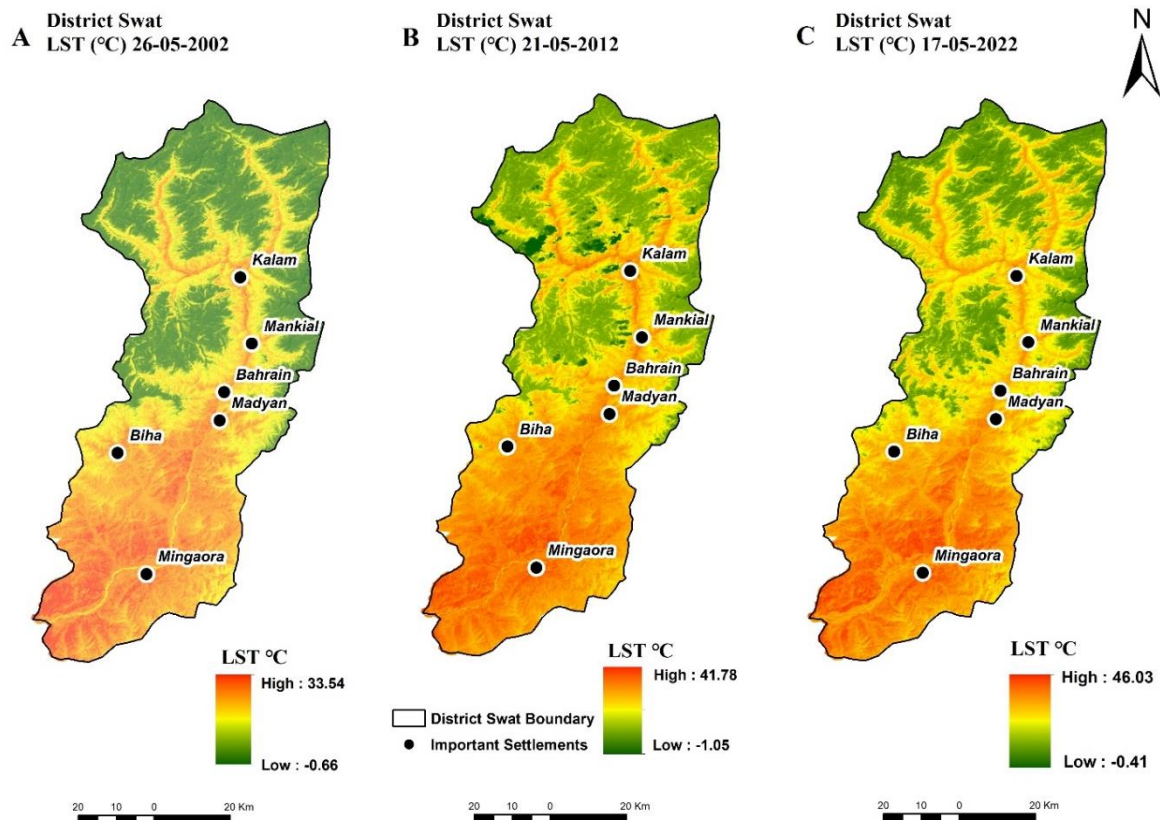


Figure 4A Shows the LST of 2002, 4B illustrates the LST of 2012, and 4C highlights the LST of 2022 of district Swat.

Table 6 Maximum, Minimum, and Mean LST of district Swat between 2002 and 2022

Year	2002	2012	2022	LST change (2002-2022)
Maximum LST (°C)	33.54	41.78	46.03	12.49
Minimum LST (°C)	-0.66	-1.05	-0.41	0.25
Mean LST (°C)	16.44	20.36	22.81	6.37

Relationship between LST and LULC Conversion

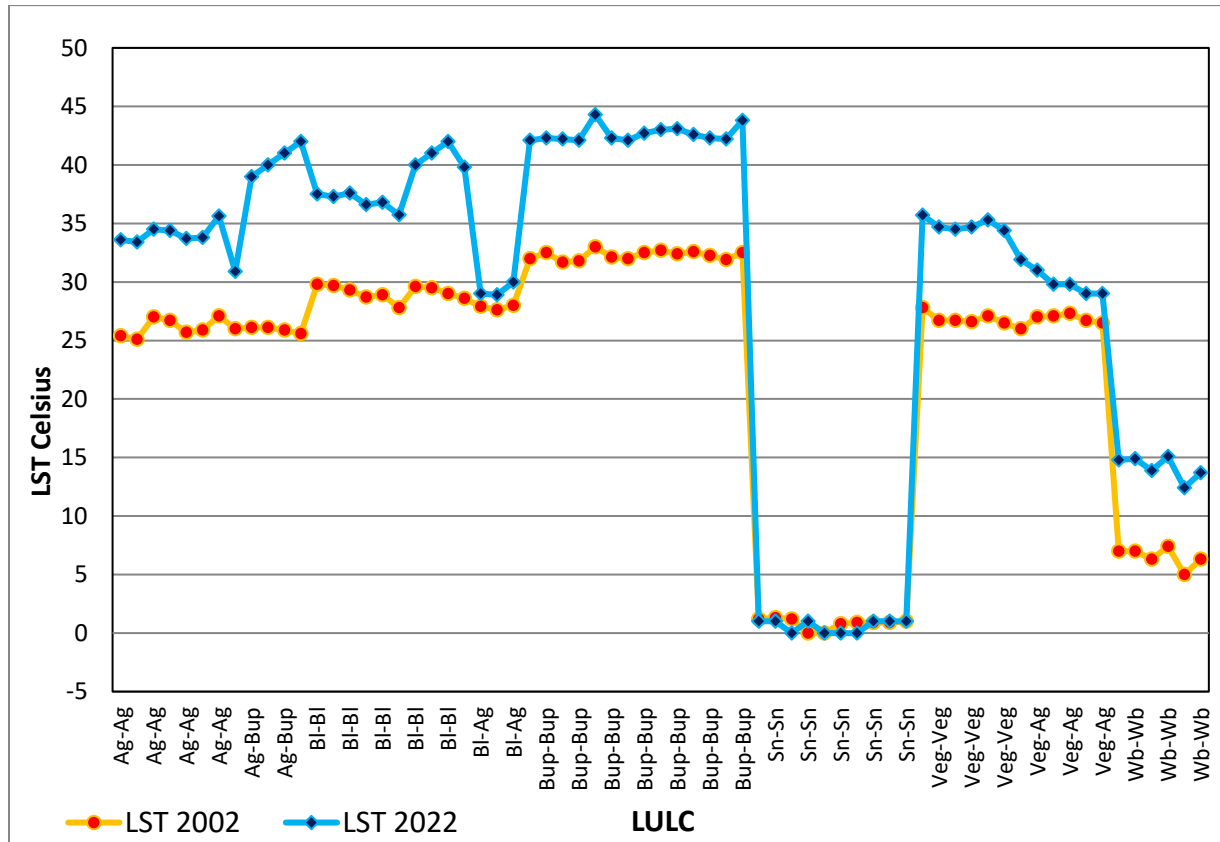
Land surface heating is the cumulative effect of LULC change on global atmospheric warming. The decline of vegetation cover driven by agricultural expansion in the study area substantially increases LST. Results show that higher LST values are recorded when vegetation cover and agricultural land converted into other land uses (Table 7). According to the analysis, changes in LULC have a significant impact on LST. For instance, the average LST was increased by 10.1°C when agricultural land was converted to the built-up area during the study period (2002 - 2022). Similarly, barren land was converted to a built-up area, as a result, the LST increased to 8.4 °C from 2002 - 2022. The agricultural land increased in 2022 by converting the barren land of 2002, hence the average LST also changed to 1.2 °C. Moreover, the average LST also rises to 3 °C by converting vegetation cove to agricultural land. Finally, the study reveals that the least change in LST 1.2 °C was reported when barren land was converted to agricultural land, while the largest LST 10. 1 °C is found when agricultural land is changed to built-up areas.

Table 7 LULC Change (2002-2022) and Corresponding LST from (2002-2022)

S.No	LULC 2002	LULC 2022	LST 2002	LST 2012	LST 2022	Change 2002-22
------	-----------	-----------	----------	----------	----------	----------------

1	Agricultural Land	Agricultural Land	25.70	30.30	33.70	8.00
2	Agricultural Land	Agricultural Land	25.90	30.40	33.80	7.90
3	Agricultural Land	Agricultural Land	27.10	31.60	35.62	8.52
4	Agricultural Land	Agricultural Land	26.00	27.50	30.90	4.90
5	Agricultural Land	Built-Up	26.10	30.60	39.00	12.90
6	Agricultural Land	Built-Up	26.10	30.60	40.00	13.90
7	Agricultural Land	Built-Up	25.90	30.40	41.00	15.10
8	Agricultural Land	Built-Up	25.60	30.10	42.00	16.40
9	Barren Land	Barren Land	29.70	34.20	37.30	7.60
10	Barren Land	Barren Land	29.30	34.20	37.60	8.30
11	Barren Land	Barren Land	28.70	33.20	36.60	7.90
12	Barren Land	Barren Land	28.90	33.40	36.80	7.90
13	Barren Land	Built-Up	29.60	34.10	40.00	10.40
14	Barren Land	Built-Up	29.50	34.00	41.00	11.50
15	Barren Land	Built-Up	29.00	33.50	42.00	13.00
16	Barren Land	Built-Up	28.60	33.10	39.80	11.20
17	Barren Land	Agricultural Land	27.90	32.40	29.00	1.10
18	Barren Land	Agricultural Land	27.60	32.10	28.90	1.30
19	Barren Land	Agricultural Land	28.00	32.50	30.00	2.00
20	Built-Up	Built-Up	32.00	38.90	42.10	10.10
21	Built-Up	Built-Up	32.50	38.90	42.30	9.80
22	Built-Up	Built-Up	31.70	38.80	42.20	10.50
23	Built-Up	Built-Up	31.80	38.70	42.10	10.30
24	Snow	Snow	1.20	0.00	1.00	-0.20
25	Snow	Snow	1.30	-1.00	1.00	-0.30
26	Snow	Snow	1.20	-1.00	0.00	-1.20
27	Snow	Snow	0.00	-1.00	1.00	1.00
28	Vegetation	Vegetation	27.80	32.30	35.70	7.90
29	Vegetation	Vegetation	26.70	31.30	34.70	8.00
30	Vegetation	Vegetation	26.70	31.20	34.50	7.80
31	Vegetation	Vegetation	26.60	31.30	34.70	8.10
32	Vegetation	Agricultural Land	27.00	31.50	31.00	4.00
33	Vegetation	Agricultural Land	27.10	31.60	29.80	2.70
34	Vegetation	Agricultural Land	27.30	31.80	29.80	2.50
35	Vegetation	Agricultural Land	26.70	31.20	29.00	2.30
36	Water Bodies	Water Bodies	7.00	11.50	14.80	7.80
37	Water Bodies	Water Bodies	7.00	11.50	14.90	7.90
38	Water Bodies	Water Bodies	6.30	10.50	13.90	7.60
39	Water Bodies	Water Bodies	7.40	11.60	15.10	7.70





5.7 Conclusion

In this research, an analysis of the impact of LULC dynamics on LST using geospatial methods in district Swat was examined. For this purpose, the Landsat datasets have been considered to examine LULC changes and monitor the LST of the study area from 2002-2022. The analysis found that agricultural land dominates all LULC classes, which is grown by 540.2 km² followed by build-up area raised by 513 km² during the study period. The main factor is the increase of agricultural land and built-up areas, as well as the decline of vegetative land and snow cover. During the study period, around 808.8 km² of vegetative land and 613.6 km² of snow cover were converted to agricultural land, built-up area, and other land uses.

The highest temperature was calculated at 33.54 °C, 41.78 °C and 46.03 °C for the years 2002, 2012, and 2022 respectively, while the low temperature was found -0.66 °C, -1.05 °C and -

0.41 respectively for the years 2002, 2012 and 2022. The southern part of the district experienced high temperatures due to the built-up environment, whereas the north-eastern and north-western parts of the study area recorded low temperatures because of the presence of vegetation and snow cover. Thus we conclude that unplanned and unauthorized built-up areas and degradation of vegetation cover are key factors in increasing LST in the study area.

References

- Abebe, M. S., Derebew, K. T., & Gemed, D. O. (2019). Exploiting temporal-spatial patterns of informal settlements using GIS and remote sensing technique: a case study of Jimma city, Southwestern Ethiopia. *Environmental Systems Research*, 8(1), 1-11.
- Alves, E. D. L. (2016). Seasonal and spatial variation of surface urban heat island intensity in a small urban agglomerate in Brazil. *Climate*, 4(4), 61.
- How Jin Aik, D., Ismail, M. H., & Muharam, F. M. (2020). Land use/land cover changes and the relationship with land surface temperature using Landsat and MODIS imageries in Cameron Highlands, Malaysia. *Land*, 9(10), 372.
- Chen, X., & Zhang, Y. (2017). Impacts of urban surface characteristics on spatiotemporal pattern of land surface temperature in Kunming of China. *Sustainable Cities and Society*, 32, 87-99.
- Congalton, R. G. (1991). A review of assessing the accuracy of classifications of remotely sensed data. *Remote sensing of environment*, 37(1), 35-46.
- Disperati, L., & Virdis, S. G. P. (2015). Assessment of land-use and land-cover changes from 1965 to 2014 in Tam Giang-Cau Hai Lagoon, central Vietnam. *Applied Geography*, 58, 48-64.
- Dutta, R. (2015). Remote sensing of energy fluxes and soil moisture content.
- Ebabu, K., Tsunekawa, A., Haregeweyn, N., Adgo, E., Meshesha, D. T., Aklog, D., Masunaga, T., Tsubo, M., Sultan, D., & Fenta, A. A. (2019). Effects of land use and sustainable land management practices on runoff and soil loss in the Upper Blue Nile basin, Ethiopia. *Science of the Total Environment*, 648, 1462-1475.
- Elias, E., Seifu, W., Tesfaye, B., & Girmay, W. (2019). Impact of land use/cover changes on lake ecosystem of Ethiopia central rift valley. *Cogent Food & Agriculture*, 5(1), 1595876.
- Feng, R., Du, Q., Li, X., & Shen, H. (2019). Robust registration for remote sensing images by combining and localizing feature-and area-based methods. *ISPRS Journal of Photogrammetry and Remote Sensing*, 151, 15-26.
- Guha, S., & Govil, H. (2020). Land surface temperature and normalized difference vegetation index relationship: a seasonal study on a tropical city. *SN Applied Sciences*, 2(10), 1661.
- Guha, S., Govil, H., Dey, A., & Gill, N. (2020). A case study on the relationship between land surface temperature and land surface indices in Raipur City, India. *Geografisk Tidsskrift-Danish Journal of Geography*, 120(1), 35-50.
- Islam, K., Jashimuddin, M., Nath, B., & Nath, T. K. (2018). Land use classification and change detection by using multi-temporal remotely sensed imagery: The case of Chunati wildlife sanctuary, Bangladesh. *The Egyptian Journal of Remote Sensing and Space Science*, 21(1), 37-47.

- Kedir, M., Schmidt, E., & Wagas, A. (2016). *Pakistan's changing demography: urbanization and peri-urban transformation over time* (Vol. 39). Intl Food Policy Res Inst.
- Khan, I., Khan, S. U., Zhao, M., & Khan, A. A. (2019). Exploring the spatial heterogeneity of individual preferences for integrated river basin management: an example of Heihe river basin. *Environmental Science and Pollution Research*, 26, 6911-6921.
- Kumar, D., & Shekhar, S. (2015). Statistical analysis of land surface temperature–vegetation indexes relationship through thermal remote sensing. *Ecotoxicology and environmental safety*, 121, 39-44.
- Liu, H., Huang, B., Zhan, Q., Gao, S., Li, R., & Fan, Z. (2021). The influence of urban form on surface urban heat island and its planning implications: evidence from 1288 urban clusters in China. *Sustain Cities Soc* 71: 102987. In.
- Mishra, P. K., Rai, A., & Rai, S. C. (2020). Land use and land cover change detection using geospatial techniques in the Sikkim Himalaya, India. *The Egyptian Journal of Remote Sensing and Space Science*, 23(2), 133-143.
- Mohajerani, A., Bakaric, J., & Jeffrey-Bailey, T. (2017). The urban heat island effect, its causes, and mitigation, with reference to the thermal properties of asphalt concrete. *Journal of environmental management*, 197, 522-538.
- Moisa, M. B., Dejene, I. N., Merga, B. B., & Gemed, D. O. (2022). Impacts of land use/land cover dynamics on land surface temperature using geospatial techniques in Anger River Sub-basin, Western Ethiopia. *Environmental Earth Sciences*, 81(3), 99.
- Msofe, N. K. (2019). Socio-ecological drivers of land use change and Wetland Conversion in Kilombero Valley Floodplain, Tanzania. *American Journal of Environmental and Resource Economics*, 4(1), 1-11.
- Namugize, J. N., Jewitt, G., & Graham, M. (2018). Effects of land use and land cover changes on water quality in the uMngeni river catchment, South Africa. *Physics and Chemistry of the Earth, Parts a/b/c*, 105, 247-264.
- Nasir, M. J., Ahmad, W., Iqbal, J., Ahmad, B., Abdo, H. G., Hamdi, R., & Bateni, S. M. (2022). Effect of the urban land use dynamics on land surface temperature: A case study of kohat city in Pakistan for the period 1998–2018. *Earth Systems and Environment*, 6(1), 237-248.
- Negash, D. A., Moisa, M. B., Merga, B. B., Sedeta, F., & Gemed, D. O. (2021). Soil erosion risk assessment for prioritization of sub-watershed: the case of Chogo Watershed, Horo Guduru Wollega, Ethiopia. *Environmental Earth Sciences*, 80(17), 589.
- Ogunode, A., & Akombelwa, M. (2017). An algorithm to retrieve land surface temperature using Landsat-8 dataset. *South African Journal of Geomatics*, 6(2), 262-276.
- Olika, G., & Iticha, B. (2019). Assessment of soil erosion using RUSLE and GIS techniques: A case of Fincha'a Watershed, Western Ethiopia. *American-Eurasian Journal of Agricultural & Environmental Sciences*, 19(1), 31-36.
- Patra, S., Sahoo, S., Mishra, P., & Mahapatra, S. C. (2018). Impacts of urbanization on land use/cover changes and its probable implications on local climate and groundwater level. *Journal of urban management*, 7(2), 70-84.
- Pouliot, D., Latifovic, R., Zabcic, N., Guindon, L., & Olthof, I. (2014). Development and assessment of a 250 m spatial resolution MODIS annual land cover time series (2000–2011) for the forest region of Canada derived from change-based updating. *Remote Sensing of Environment*, 140, 731-743.

- Qasim, M., Hubacek, K., Termansen, M., & Fleskens, L. (2013). Modelling land use change across elevation gradients in district Swat, Pakistan. *Regional environmental change*, 13, 567-581.
- Qasim, M., Hubacek, K., Termansen, M., & Khan, A. (2011). Spatial and temporal dynamics of land use pattern in District Swat, Hindu Kush Himalayan region of Pakistan. *Applied Geography*, 31(2), 820-828.
- Rahaman, S., Kumar, P., Chen, R., Meadows, M. E., & Singh, R. (2020). Remote sensing assessment of the impact of land use and land cover change on the environment of Bardhaman district, West Bengal, India. *Frontiers in Environmental Science*, 8, 127.
- Rajendran, P., & Mani, K. (2015). Estimation of spatial variability of land surface temperature using Landsat 8 imagery. *International Journal of Engineering and Science*, 11(4), 19-23.
- Rani, N., Mandla, V. R., & Singh, T. (2017). Evaluation of atmospheric corrections on hyperspectral data with special reference to mineral mapping. *Geoscience Frontiers*, 8(4), 797-808.
- Song, X.-P., Hansen, M. C., Stehman, S. V., Potapov, P. V., Tyukavina, A., Vermote, E. F., & Townshend, J. R. (2018). Global land change from 1982 to 2016. *Nature*, 560(7720), 639-643.
- Tan, J., Yu, D., Li, Q., Tan, X., & Zhou, W. (2020). Spatial relationship between land-use/land-cover change and land surface temperature in the Dongting Lake area, China. *Scientific Reports*, 10(1), 9245.
- Tezera, A., Chanie, T., Feyisa, T., & Jemal, A. (2015). Impact assessment of land use/land cover change on soil erosion and rural livelihood in Andit Tid Watershed, North Shewa, Ethiopia. *Archives of Current Research International*, 3(1), 1-10.
- Tomar, V., Kumar, P., Rani, M., Gupta, G., & Singh, J. (2013). A satellite-based biodiversity dynamics capability in tropical forest. *Electron. J. Geotech. Eng*, 18, 1171-1180.
- Zhou, F., & Zhong, D. (2020). Kalman filter method for generating time-series synthetic Landsat images and their uncertainty from Landsat and MODIS observations. *Remote Sensing of Environment*, 239, 111628.
- Zou, F., Li, H., & Hu, Q. (2020). Responses of vegetation greening and land surface temperature variations to global warming on the Qinghai-Tibetan Plateau, 2001–2016. *Ecological Indicators*, 119, 106867.